BMC Microbiology

RESEARCH

Open Access

Pulmonary metabolic changes in a rabbit model of *Pseudomonas aeruginosa* pneumonia: insights from metabolomic analysis

Fuzhi Lai[1†], Zhibin Zhou[2†], Xiaojiao Xia[2†], Yuxia Du[3*] and Jiaming Huang[4]

Abstract

Background The current problem associated with *Pseudomonas aeruginosa* (PA) pneumonia, which is frequently encountered in clinical settings, is drug resistance. If *Pseudomonas aeruginosa* pneumonia can be rapidly diagnosed in early stage, the occurrence of drug resistance can be reduced. Therefore, our study aimed to investigate pulmonary metabolic changes associated with PA pneumonia and to identify relevant metabolic biomarkers and key metabolic pathways, providing a reference for rapid diagnosis.

Methods Eighteen rabbits were randomly assigned to either the PA or normal saline (NS) group. Bronchoalveolar lavage fluid (BALF) was analyzed via untargeted liquid chromatography-mass spectrometry (ULCMS) to identify and analyze differentially abundant metabolites between the groups. Univariate comparisons were performed using Student's t-test, while multivariate patterns were analyzed via principal component analysis (PCA) and orthogonal projections to latent structure-discriminant analysis(OPLS-DA).

Results Successful modeling was achieved in 17 rabbits (8 PAs, 9 NSs). The most abundant metabolite classes detected in BALF were lipids and lipid-like molecules, organoheterocyclic compounds, and benzenoids. A total of 2,451 differentially abundant metabolites were identified, including 1,205 upregulated and 1,210 downregulated metabolites. Key metabolic pathways such as histidine metabolism, arginine and proline metabolism, nucleotide metabolism, and ABC transporters were upregulated in the PA group, whereas choline metabolism in the cancer pathway was downregulated.

Conclusion PA pneumonia induces distinctive metabolic alterations in the lungs, highlighting potential biomarkers and pathways that could provide valuable insights for clinical diagnosis and treatment.

Clinical trial number Not applicable.

Keywords Pseudomonas aeruginosa pneumonia, Metabolomic analysis, Bronchoalveolar lavage fluid (BALF)

† Fuzhi Lai, Zhibin Zhou and Xiaojiao Xia have contributed equally to this work.

*Correspondence:
Yuxia Du
yuxia-du@fjmu.edu.cn

Full list of author information is available at the end of the article

Introduction

Pneumonia is a prevalent acute respiratory infection associated with high morbidity and mortality rates globally. In 2021, there were an estimated 344 million cases of lower respiratory tract infections, resulting in 2.18 million deaths [1]. *Pseudomonas aeruginosa* (PA) is a frequent causative agent of pneumonia. Current antibiotic treatments for PA infections face substantial challenges, particularly due to the emergence of drug-resistant strains. As early as 2017, the World Health Organization identified carbapenem-resistant PAs as a critical priority for new antibiotics [2]. In recent years, the incidence of multidrug-resistant (MDR) and extensively drug-resistant (XDR) PAs has been increasing globally [3, 4]. PA is a common pathogen in severe infections, ranking fourth among the most common pathogens associated with severe community-acquired pneumonia in China [5].

Metabolomic analysis, which focuses on the qualitative and quantitative profiling of small molecule metabolites in body fluids, provides valuable insights into the production of and changes in endogenous metabolites under various pathophysiological conditions. Metabolites, which are located downstream of genes and proteins, provide a comprehensive view of organisms' responses to external stimuli and pathological changes. By employing pattern recognition methods, metabolomics enables the systematic study of low-molecular-weight metabolites, facilitating the comparison of differences between populations and the identification of disease-specific biomarkers. Different pathogens induce distinct biological metabolites and metabolic characteristics; unique biomarkers related to biological metabolism have been reported for PA infections [6]. Investigating metabolic changes in the lungs during PA pneumonia has the potential for early diagnosis and treatment strategies, ultimately improving patient prognosis.

Previous studies have demonstrated that untargeted metabolomics analysis, particularly untargeted liquid chromatography-mass spectrometry (ULCMS), can effectively distinguish and characterize PA infections with varying virulence and biofilm phenotypes, offering clinical utility in identifying PA infections [7]. Additionally, ULCMS detection can elucidate metabolic pathway variances in PA infections, providing insights into biofilm formation models and aiding in biofilm control [8, 9]. Despite these advancements, research on ULCMS analysis of bronchoalveolar lavage fluid (BALF) in PA pneumonia remains limited. Therefore, our study aims to conduct ULCMS analysis of metabolites in BALF from PA pneumonia models to further elucidate the metabolic characteristics of PA infections, identify potential metabolic biomarkers and key pathways, and explore novel therapeutic targets.

Materials and methods

Experimental animals and bacteria

Eighteen healthy male New Zealand white rabbits, aged 8–9 months and weighing 2–3 kg, were obtained from the Animal Laboratory of Quanzhou Medical College. The rabbits were randomly allocated to the PA group ($n = 9$) or the NS group ($n = 9$) via a computer-generated randomization sequence. The rabbits were individually housed in standardized cages and provided with a regular diet consisting of ad libitum water and fresh vegetables. They were maintained under controlled environmental conditions, with a temperature of 23 ± 2 °C and a relative humidity of 45–55%. Prior to the experiments, the rabbits were acclimatized to the facility for one week. The PA standard strain (ATCC 27853) was cultured on agar plates, and colonies were selected for the preparation of a bacterial suspension. The suspension was then diluted with physiological saline to a concentration of 3×10^8 CFU/ml. All animal care and experimental procedures were conducted in strict adherence to the institutional guidelines and national regulatory standards and were formally approved by the Medical Ethics Committee of the Second Affiliated Hospital of Fujian Medical University (Ethics Approval No. 2021 – 155).

Main experimental reagents and instruments

Methanol, acetonitrile, ammonium acetate, and ammonium hydroxide were obtained from commercial suppliers. The study utilized an ELISA reader (Dynex Technologies, Guangdong), an ultrahigh-performance liquid chromatography system (Vanquish, Thermo Fisher Scientific), a high-resolution mass spectrometer (Orbitrap Exploris 120, Thermo Fisher Scientific), and a centrifuge (Heraeus Fresco17, Thermo Fisher Scientific).

Establishment of the pneumonia model

The rabbits were placed in a prone position and anesthetized with a combination of Zoletil and xylazine 15 min prior to the procedure. Surgical procedures were performed by a dedicated operator blinded to the experimental groups. Using sterile techniques, the operator performed endotracheal intubation and inserted a drainage tube into the lower bronchus of the rabbit. A bacterial suspension containing 3×10^8 CFU/mL PA was injected (1.5 mL) into the lower bronchi of the rabbits in the PA group, whereas those in the control group received 1.5 mL of saline (Fig. 1).

Postinfection, all rabbits were subjected to three daily clinical evaluations, which included an assessment of coughing episodes, respiratory patterns, activity levels, and food consumption. Body temperature was recorded three times daily via a clinical thermometer. The rabbits were also observed daily for signs of coughing, respiratory condition, activity levels, and food intake. Three days

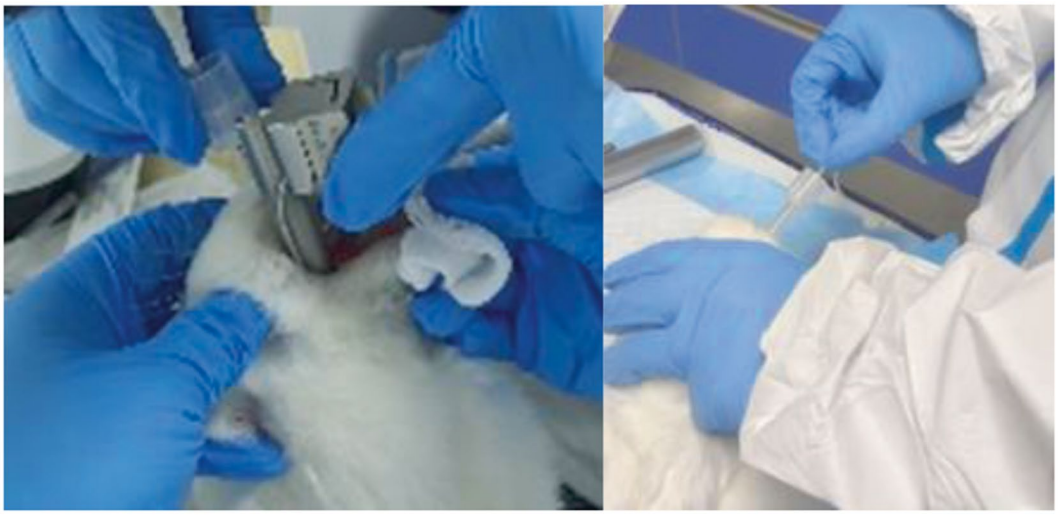

Fig. 1 Surgical procedures for establishing the PA pneumonia model. (**A**) Endotracheal intubation of a rabbit; (**B**) Insertion of a drainage tube into the lower bronchus

after bacterial injection, X-ray imaging was performed to assess lung shadows, lung lesions, and pneumonia in the rabbits. After 3 days of intervention, euthanasia was performed via the injection of Zoletil (10 mg/kg) and potassium chloride (1 g/kg). Humane endpoints were maintained throughout the study to minimize suffering. Rabbits exhibiting severe distress or health deterioration were promptly euthanized in accordance with ethical guidelines. Animals demonstrating critical morbidity indicators requiring euthanasia include the following: (1) severe respiratory distress, which is unresponsive to treatment; (2) neurological signs (e.g., persistent convulsions, persistent circling, paresis/paralysis) that interfere with eating and drinking and from which recovery is unlikely; and (3) a combination of the following: poor physical appearance (very rough hair coat, abnormal posture, grunting on exhalation); abnormal behavior (reduced mobility/unconsciousness, unsolicited vocalizations, self-mutilation); severe depression or abnormal/exaggerated responses to external stimuli; and persistent hypothermia/complete anorexia. All procedures were conducted by trained personnel in accordance with animal welfare and research protocols.

Under strict aseptic conditions, BALF was collected from each rabbit to prevent contamination. The rabbits were intubated with a sterile endotracheal catheter, and one lung was ligated at the hilum for isolation. The contralateral lung was lavaged via pre-sterilized equipment by slowly instilling sterile saline at 4 °C through the tracheal catheter. After a 30-second dwell time to ensure adequate contact between the saline and alveolar surfaces, the fluid was gently aspirated into a sterile collection tube. This lavage cycle (5 mL of saline per cycle) was repeated three times to maximize alveolar content recovery. All instruments, including endotracheal catheters and collection tubes, were autoclaved prior to use, while operators wore sterile gloves, masks, and gowns to minimize contamination risks. Immediately after collection, the BALF was placed on ice to inhibit microbial growth. The samples were centrifuged to separate the supernatant, which was aliquoted into sterile cryovials and stored at − 80 °C for subsequent analysis. BALF from both groups was analyzed via untargeted metabolomics.

Untargeted metabolomics analysis and data processing

Blinding procedures were rigorously implemented throughout the metabolite extraction, instrumental analysis, and data processing phases. All personnel involved in the LC-MS/MS operation and data interpretation were blinded to the group allocation until the completion of the statistical analysis.

Metabolite extraction from BALF

A 100 μL aliquot of each sample was mixed with 400 μL of extraction solution (MeOH: ACN, 1:1 (v/v)), which contained deuterated internal standards. The mixed solution was vortexed for 30 s, sonicated for 10 min in a 4 °C water bath, and incubated for 1 h at -40 °C to precipitate the proteins. The samples were then centrifuged at 12,000 rpm (RCF = 13800×g, R = 8.6 cm) for 15 min at 4 °C. The supernatant was transferred to a fresh glass

vial for analysis. The QC sample was prepared by mixing equal aliquots of the supernatant of the samples.

LC-MS/MS analysis

For polar metabolites, LC-MS/MS analyses were performed via an ultrahigh-performance liquid chromatography (UHPLC) system (Vanquish, Thermo Fisher Scientific) equipped with a Waters ACQUITY UPLC BEH amide column (2.1 mm × 50 mm, 1.7 μm) coupled to an Orbitrap Exploris 120 mass spectrometer (Orbitrap MS, Thermo). The mobile phase consisted of 25 mmol/L ammonium acetate and 25 mmol/L ammonia hydroxide in water (pH = 9.75) (A) and acetonitrile (B). The autosampler temperature was maintained at 4 °C, and the injection volume was 2 μL. The Orbitrap Exploris 120 mass spectrometer was used for its ability to acquire MS/MS spectra in information-dependent acquisition (IDA) mode under the control of acquisition software (Xcalibur, Thermo). In this mode, the acquisition software continuously evaluates the full-scan MS spectrum. The ESI source conditions were set as follows: sheath gas flow rate, 50 Arb; aux gas flow rate, 15 Arb; capillary temperature, 320 °C; full MS resolution, 60,000; MS/MS resolution, 15,000; collision energy, SNCE 20/30/40; and spray voltage, 3.8 kV (positive) or -3.4 kV (negative).

Data preprocessing and annotation

The raw data were converted to mzXML format via ProteoWizard and processed with an in-house program developed via R and XCMS for peak detection, extraction, alignment, and integration. Metabolite identification was performed via BiotreeDB (V3.0) with enhanced spectral matching, where the detected metabolites were annotated by matching the retention time (RT), precursor ion mass-charge ratio (MS1), and tandem mass spectral patterns (MS2) against the upgraded local database. Metabolite identifications were annotated according to confidence levels defined by the Metabolomics Standards Initiative (MSI) [10].

Level 1: Matches with authentic standards in MS1, MS2, and retention time (RT);

Level 2: Matches in MS1 and MS2 with public spectral databases;

Level 3: Matches with compounds in MS1, MS2, and RT;

Level 4: Unknown compounds.

The R package was applied for subsequent data processing [11].

The data were normalized and analyzed by clustering heatmaps and principal component analysis (PCA) to identify uncorrelated variables. Statistical analysis was performed with orthogonal projections to latent structure-discriminant analysis (OPLS-DA), with model robustness assessed via 7-fold cross-validation. Significantly altered metabolites were identified on the basis of variable importance in the projection (VIP) values > 1 and P values < 0.05. Metabolic regulation was further examined via volcano plots.

Statistical analysis

Continuous data are presented as the means ± standard deviations (SDs), whereas categorical variables are described as numbers (percentages). For univariate statistical analysis, the Student's *t*-test was conducted for intergroup comparisons, with false discovery rate (FDR) control implemented via the Benjamini-Hochberg (BH) method for *P*-value correction. Multivariate statistical analyses included PCA and OPLS-DA, among others, to explore complex relationships within the data. Model validation was performed via methods such as 7-fold cross-validation. A two-tailed *P*-value < 0.05 was considered statistically significant, indicating strong evidence against the null hypothesis.

Results

General characteristics

A total of nine rabbits were included in the experimental group to establish a PA pneumonia model. On day 2 post-modeling, a rabbit demonstrated unresponsiveness to environmental stimuli, hypothermia (rectal temperature < 35 °C), and persistent complete anorexia. Despite the implementation of supportive care measures, which included maintenance of body temperature and fluid replacement therapy, the condition of the animal did not stabilize. The anticipated death became inevitable. To further alleviate suffering, the animal was humanely euthanized via the injection of Zoletil and potassium chloride. Postmortem histopathological examination confirmed that the definitive cause of the disease was suppurative pneumonia. During the observation period, the body temperatures of the rabbits in the model group were greater than those in the control group on days 1, 2, and 3, although these differences were not statistically significant ($P > 0.05$).

Quality control and cluster analysis

The quality of the samples analyzed by chromatography was satisfactory, the experimental methods were robust, and the system stability was excellent. The retention time and response intensity of the internal standards in the QC samples demonstrated good stability, and the instrument data acquisition was consistent. No significant peaks of internal standards were detected in the blank samples, indicating effective control of cross-contamination. The QC samples exhibited excellent homogeneity, confirming the stability of the experimental methods. Furthermore, the QC samples showed good clustering in the two-dimensional PCA score plot, indicating high method

stability. Furthermore, all the QC samples fell within ± 2 standard deviations in the PCA-X one-dimensional distribution plot, reflecting high data quality (Fig. 2).

PCA and OPLS-DA

The PCA score plot showed tight clustering of the QC samples, indicating excellent method stability and aggregation. Distinct separation was observed between the PA and NS groups, highlighting significant differences in their metabolite profiles. This separation was further corroborated by OPLS-DA, which demonstrated robust discrimination between the experimental conditions (Fig. 3).

Differentially abundant metabolite analysis

A total of 2,451 differentially abundant metabolites were identified across all the samples, including 1,205 upregulated and 1,210 downregulated metabolites. These differences are visually represented in volcano plots, which depict the variations in metabolite levels between the PA and NS groups (Fig. 4).

The significantly elevated metabolites included PE(P-18:1(9Z)/18:1(9Z)), hexanedioic acid, pentanedioic acid, 3-methylhistidine, and 3beta-hydroxyandrosta-5,15-dien-17-one. Conversely, notable decreases were observed in LPE(14:0), palmitoylglycerone phosphate, and lysoPE(0:0/18:0). These significant changes are visually represented in the volcano plot (Fig. 5).

Kyoto encyclopedia of genes and genomes (KEGG) pathway enrichment analysis of differentially abundant metabolites

Bioinformatic analysis revealed abnormalities in 10 metabolic pathways, including amino acid metabolism, cancer overview, drug resistance (antineoplastic), endocrine and metabolic diseases, global overview maps, membrane transport, metabolism of cofactors and vitamins, nucleotide metabolism, the sensory system, and signal transduction. KEGG pathway enrichment revealed 14 upregulated pathways in the model group compared with the control group, including histidine metabolism, arginine and proline metabolism, antifolate resistance, insulin resistance, nucleotide metabolism, biosynthesis of amino acids, 2-oxocarboxylic acid metabolism, metabolic pathways, ABC transporters, nicotinate and nicotinamide metabolism, pyrimidine metabolism, purine metabolism, olfactory transduction, and the cGMP-PKG signaling pathway. In contrast, choline metabolism, a cancer pathway metabolite, was downregulated.

Differential abundance (DA) score analysis revealed the upregulation of specific metabolites involved in 2-oxocarboxylic acid metabolism and metabolic pathways, whereas metabolites involved in choline metabolism among cancer pathway metabolites were downregulated. Receiver operating characteristic (ROC) curve and area under the curve (AUC) calculations confirmed high accuracy in distinguishing between the PA and NS groups. See Fig. 6 for details.

Discussion

This study utilized untargeted metabolomics to investigate changes in metabolite profiles within the bronchoalveolar lavage fluid of a PA pneumonia animal model. Untargeted metabolomics allows for the comprehensive and unbiased detection of all small-molecule metabolites in a high-throughput manner. Subsequent bioinformatics analyses were performed to identify differentially abundant metabolites and reveal the underlying physiological mechanisms of metabolic pathways. Our findings revealed elevated levels of lipids, lipid-like molecules, and benzenoids in the PA pneumonia model. Among these, PE(P-18:1(9Z)/18:1(9Z)), 3-methylhistidine, and benzenoids exhibited the strong associations with inflammation in our model. These metabolites warrant prioritization as potential biomarkers for PA pneumonia diagnosis or therapeutic monitoring. For instance, noninvasive detection of exhaled benzenoids (via breath analysis) or blood-based quantification of 3-methylhistidine could bridge translational gaps in human applications. However, the mechanistic links between these metabolic changes and the pathophysiology of PA pneumonia remain insufficiently elucidated.

We observed that the upregulation of lipids and lipid-like molecules, such as glycerophospholipids and sphingolipids, plays a critical role in cell membrane structure and function. Research has underscored the importance of lipid and lipid-like molecules—such as glycerophospholipids, fatty acyls, and sphingolipids—as key differentially abundant metabolites in pneumonia and upper respiratory tract infections [12–15]. Specifically, dysregulation of lipid metabolism has been implicated in inflammatory cell infiltration during pulmonary inflammation and immune responses and is strongly correlated with infection severity [16–18]. For example, pulmonary infections and other stress conditions stimulate the production of oxidative phospholipids in the lungs, which activate alveolar macrophages to produce reactive oxygen species, contributing to harmful proinflammatory responses and acute injury [18]. Importantly, inflammatory responses to infection involve both proinflammatory and anti-inflammatory lipid mediators [19].

Moreover, the aromatic compounds detected in our study, particularly benzenoids, could influence inflammatory responses during PA infection by modulating inflammatory signaling pathways or mediator production. Benzenoids are volatile organic compounds, and derivatives of benzene have been detected in exhaled breath under specific conditions. Notably, increases in

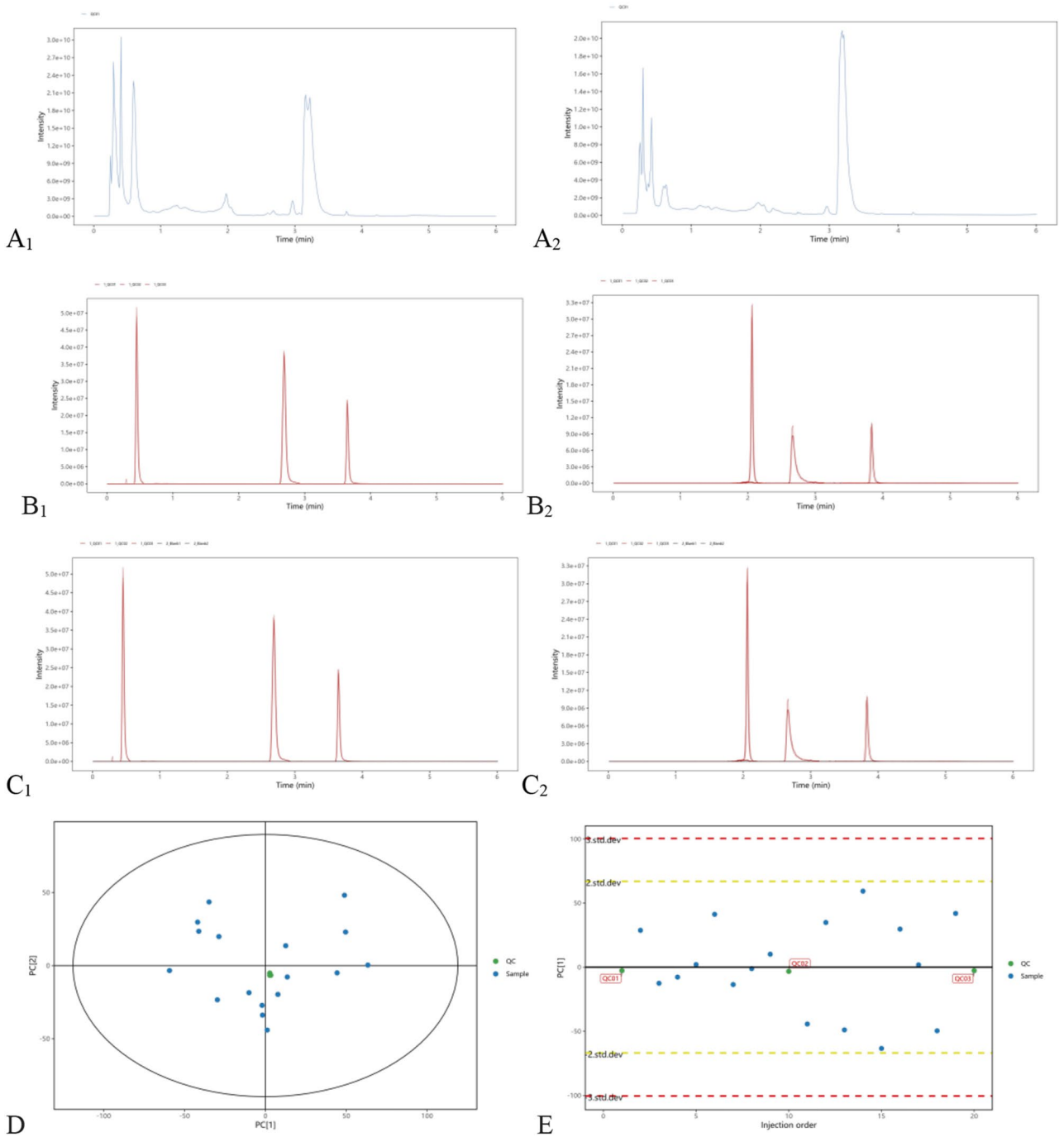

Fig. 2 Quality control validation for metabolomic analysis. (**A**)Total ion chromatograms(TIC) plot of QC samples analyzed by ultrahigh-performance liquid chromatography-orbitrap exploris-mass spectrometry (UHPLC-OE-MS): A_1(positive ion mode) and A_2 (negative ion mode); (**B**) EIC of all QC samples with internal standard: B_1 (positive ion mode) and B_2 (negative ion mode), B_1-B_2 demonstrate consistent retention time and response intensity of internal standards across QCs; (**C**) EIC plots of blank and QC samples with internal standard: C_1 (positive ion mode) and C $_2$(negative ion mode), C_1-C_2 confirm absence of detectable residues in blank samples; (**D**) Principal component analysis (PCA) score plot with tight QC clustering, showing the detection and analysis method has high stability; (**E**) Presentation of QC samples in the PCA-X one-dimensional distribution plot

certain volatile organic compounds have been reported in esophageal and gastric adenocarcinomas [20]. The elevated levels of benzenoids observed in PA infection suggest their potential as biomarkers for noninvasive monitoring or assessment of therapeutic efficacy in PA pneumonia.

Among the significantly altered metabolites, PE(P-18:1(9Z)/18:1(9Z)), 3-methylhistidine, and

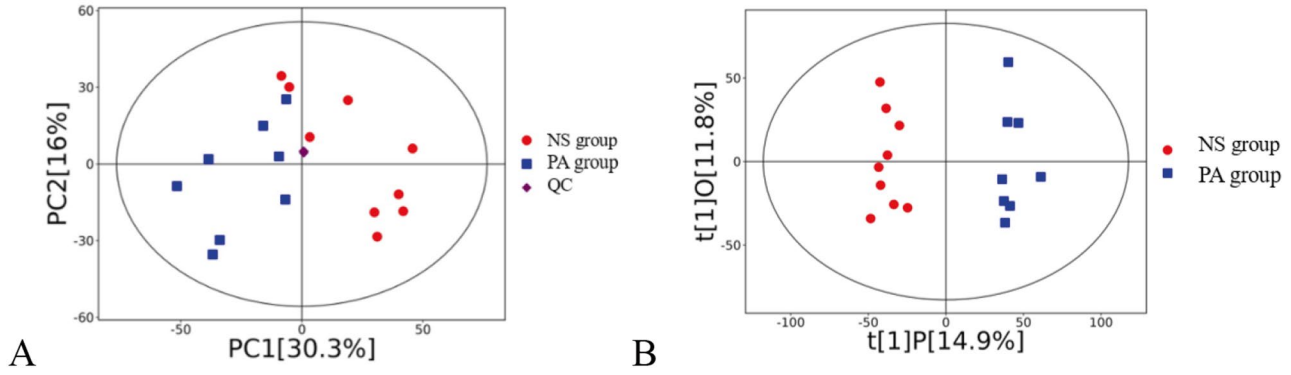

Fig. 3 Multivariate analysis revealed intergroup metabolic profile disparities. (**A**) Principal component analysis (PCA) score plot: QC samples showed tight clustering, indicating analytical stability. The PA group and NS group were distinctly separated along PC1 (30.3% variance explained). Hotelling's T^2 ellipse (95% confidence interval) confirmed that the intergroup differences exceeded random variation. (**B**) OPLS-DA validation: Model parameters $R^2Y = 0.93$ and $Q^2 = 0.58$ (200-permutation test, $P < 0.05$) demonstrated strong predictive power. The OPLS-DA score plot shows the first predictive component (t [1]P:14.9%), which explains the variation between the groups, versus the first orthogonal component (t [1]O:11.8%), which explains the variation within the groups. The PA samples clustered in the positive t [1]P[14.9%] direction, whereas the NS samples clustered in the negative direction, indicating infection-induced systemic metabolic reprogramming

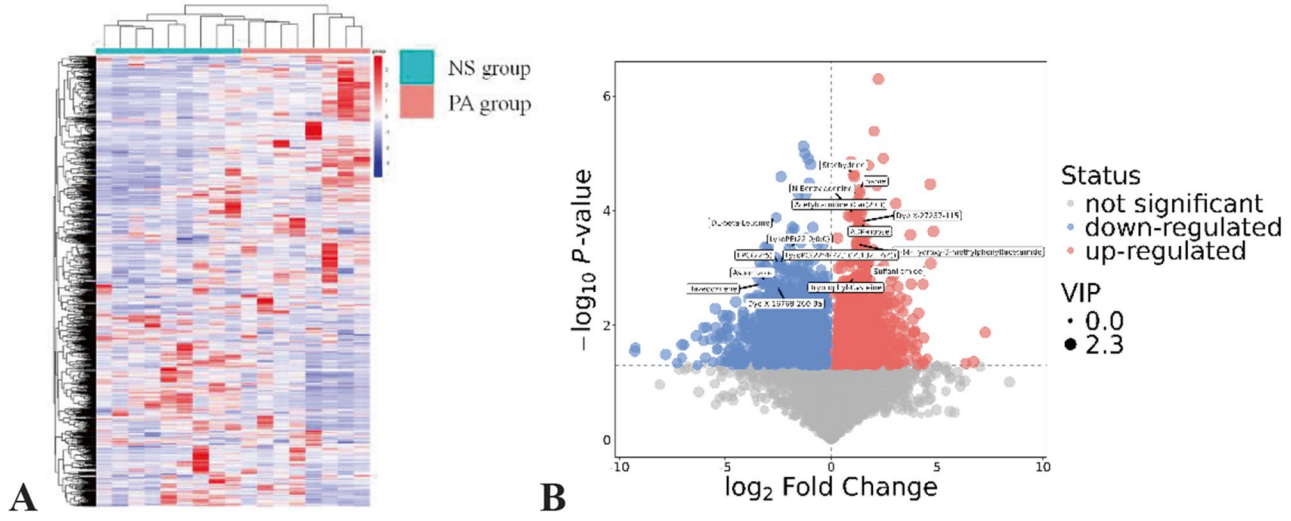

Fig. 4 Heatmap and volcano plot showing differentially abundant metabolites in BALF from PA-infected vs. control rabbits. (**A**) Sample-metabolite expression heatmap. The x-axis indicates different sample groups, and the y-axis represents all the metabolites. The color gradient represents the normalized relative abundance (red: high expression, blue: low expression). (**B**) Differentially abundant metabolite volcano plot: the x-axis shows the *log2(fold change)* of PA versus NS, and the y-axis represents -log10 adjusted *P* -values (B-Hochberg method). The significance thresholds were set at $P < 0.05$ (horizontal dashed lines)

3beta-hydroxyandrosta-5,15-dien-17-one were notably upregulated, whereas LPE(14:0) and Lysopine (0:0/18:0) were downregulated. These differentially abundant metabolites are closely associated with inflammatory responses, indicating their potential as biomarkers for diagnosing and predicting PA pneumonia. For example, PE(P-18:1(9Z)/18:1(9Z)) is a crucial phospholipid involved in maintaining biological membrane structure and stability, and elevated PE(P-18:1(9Z)/18:1(9Z)) is linked to poor prognosis in critically ill patients [21, 22]. Similarly, 3-methylhistidine (3-MH), derived from histidine methylation, serves as an inflammation severity marker and is associated with poor outcomes in acute respiratory failure patients [23–25]. Additionally, 3beta-hydroxyandrosta-5,15-dien-17-one (DHEA), a versatile steroid hormone precursor, has potential prognostic and therapeutic value in various diseases, including its role in predicting adverse outcomes in severe infections [26–29].

To further elucidate the pathogenesis of PA pneumonia, we performed the Kyoto Encyclopedia of Genes and Genomes (KEGG) pathway enrichment analysis, which revealed significant alterations in multiple metabolic pathways, including amino acid metabolism, nucleotide metabolism, and signal transduction. These changes reflect complex metabolic adaptations and immune responses in the context of infection. Notably,

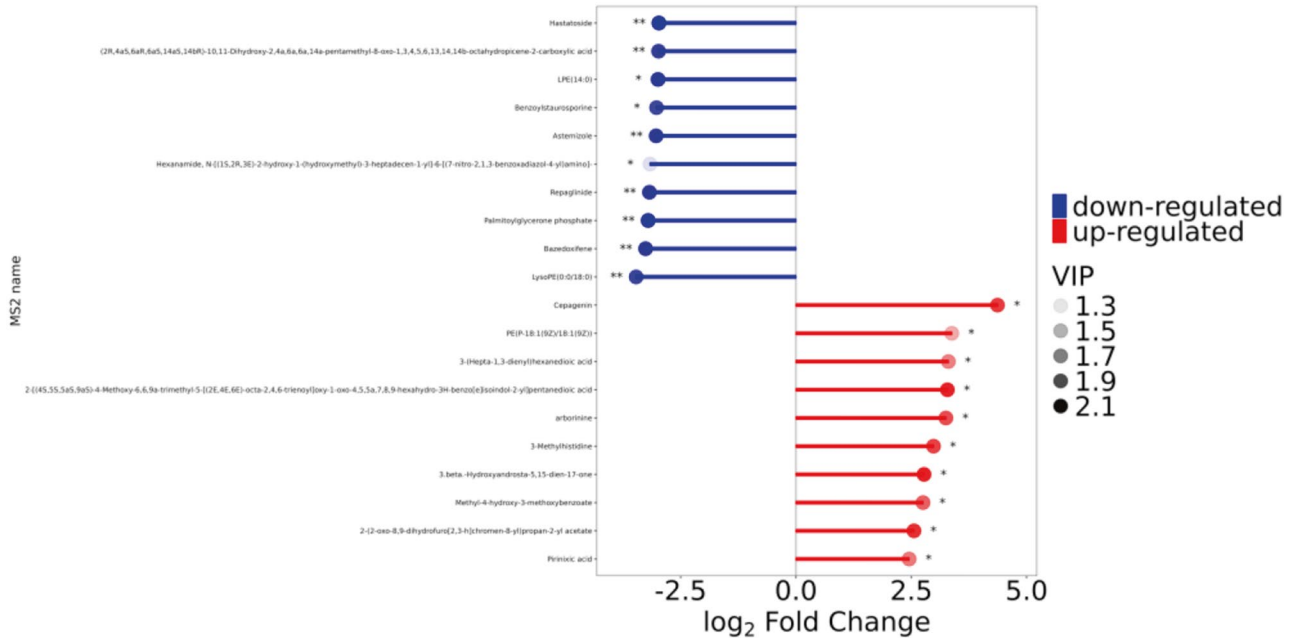

Fig. 5 The top-changed metabolites are displayed. The y-axis lists the top 10 upregulated/downregulated metabolites. Examples of metabolites included phosphatidylethanolamine (PE (P-18:1(9Z)/18:1(9Z))), which was significantly upregulated ($log_2 fold\ change = 3.38$, VIP = 1.48). * ($0.01 < P < 0.05$), ** ($0.001 < P < 0.01$), and *** ($P < 0.001$)

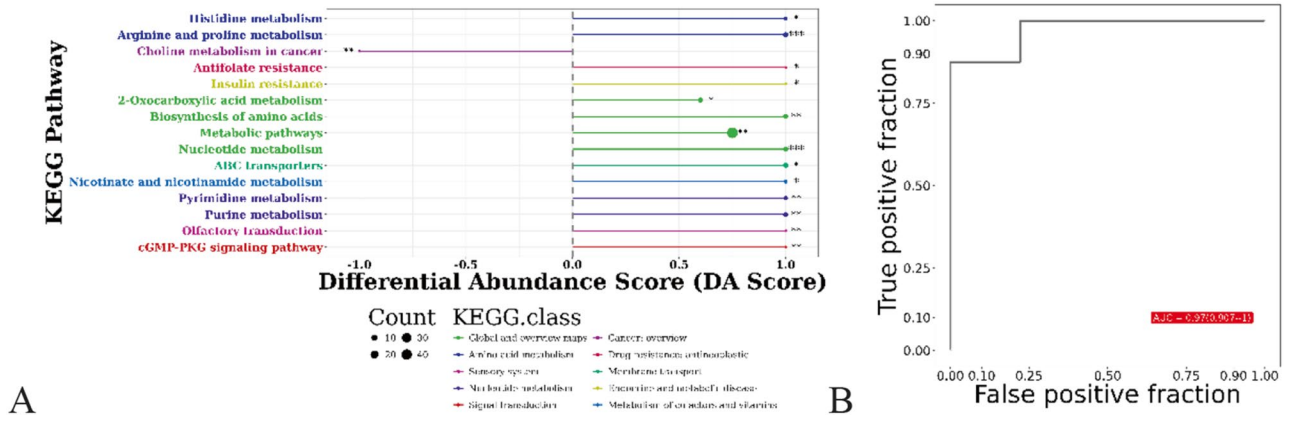

Fig. 6 KEGG pathway differential abundance scoring and metabolite diagnostic validation. (**A**) The x-axis indicates pathway-wide regulation (positive: upregulation; negative: downregulation). Bar length reflects the magnitude of the DA score. (**B**) ROC curve validation: The metabolite 1-[4-hydroxy-3-(3-methylbut-2-enyl)phenyl] ethanone demonstrated strong discriminative power for PA infection (AUC = 0.97, 95% CI: 0.907-1.0)

the increase in histidine metabolism and arginine/proline metabolism may be related to PA virulence factors and biofilm formation [30]. Furthermore, the cGMP-PKG signaling pathway, which was upregulated in our study, may be associated with airway dysfunction caused by inflammation. Previous research has suggested that nitric oxide (NO)-dependent activation of G protein-coupled receptors may impair platelet function and induce myocardial suppression through the cGMP/PKG pathway [31–33].

Despite these insights, our animal model provides controlled conditions to study PA pneumonia pathogenesis, it has inherent limitations. Rodent models cannot fully recapitulate human immune-metabolic interactions, and the single-strain PA infection protocol may oversimplify the polymicrobial dynamics observed in clinical pneumonia. Additionally, the untargeted metabolomics approach has limitations that must be acknowledged. For example, this method struggles to identify numerous unknown metabolites and may be confounded by environmental or feed-related contaminants [13]. The complexity of metabolic processes and our limited understanding of specific metabolite interactions may further complicate analysis and interpretation. For example, some metabolite changes may not be directly caused by PA infection but rather by systemic inflammatory responses or comorbidities [18]. Additionally, aromatic compounds detected

in the blood of sepsis patients may originate from either host or pathogen metabolism and play pivotal roles during infection [34]. Therefore, future studies should integrate targeted metabolomics and functional validation experiments to elucidate the links between metabolic changes and disease mechanisms more accurately. Follow-up studies integrating human patient samples (e.g., BALF from mechanically ventilated pneumonia patients) are critical to distinguish conserved metabolic signatures from model-specific artifacts.

In conclusion, our study provides a comprehensive analysis of metabolic alterations in PA pneumonia, highlighting the potential roles of lipids, benzenoids, and specific metabolic pathways in disease pathogenesis. These findings enhance our understanding of the biological and molecular mechanisms underlying PA infection and suggest potential areas for future research on therapeutic targets or biomarkers. However, the limitations of untargeted metabolomics, such as the difficulty in identifying unknown metabolites and potential confounding factors, underscore the need for further validation in larger cohorts and complementary experimental approaches.

Acknowledgements
We would like to thank Qingqing Song and Yifan Yu of Shanghai Biotree Biomedical Technology Co., Ltd. for their support with untargeted metabolomics testing and analysis technology.

Author contributions
FL and ZZ: conceptualization and writing of the original draft. XX: data curation. YD: conceptualization and funding acquisition. JH: project administration. All the authors contributed to drafting the article or critically revising it for important intellectual content, and all the authors approved the final version to be submitted.

Funding
This work was supported by the Fujian Provincial Natural Science Foundation of China (grant number: 2021J01262).

Data availability
The datasets used and analyzed during our study are available from the corresponding author on reasonable request.

Declarations

Ethics approval and consent to participate
This study was conducted in full accordance with the ethical principles of the World Medical Association's Declaration of Helsinki, and it was approved by the Medical Ethics Committee of Fujian Medical University Affiliated Second Hospital (Ethics Approval No. 2021–155). Consent to participate was not applicable.

Consent for publication
Not applicable.

Competing interests
The authors declare no competing interests.

Author details
[1]Department of Service Center, The Second Affiliated Hospital of Fujian Medical University, Quanzhou, Fujian, China
[2]Department of Respiratory and Critical Care Medicine, The Shishi Municipal Hospital, Shishi, Fujian, China
[3]Department of General Practice, The Second Affiliated Hospital of Fujian Medical University, Quanzhou, Fujian, China
[4]Microbiology Laboratory, The Second Affiliated Hospital of Fujian Medical University, Quanzhou, Fujian, China

Received: 30 March 2025 / Accepted: 20 May 2025
Published online: 28 May 2025

References

1. Global., *regional, and national incidence and mortality burden of non-COVID-19 lower respiratory infections and aetiologies, 1990–2021: a systematic analysis from the Global Burden of Disease Study 2021*. Lancet Infect Dis, 2024.
2. Tacconelli E, Carrara E, Savoldi A, et al. Discovery, research, and development of new antibiotics: the WHO priority list of antibiotic-resistant bacteria and tuberculosis. Lancet Infect Dis. 2018;18(3):318–27.
3. Horcajada JP, Montero M, Oliver A et al. Epidemiology and treatment of Multidrug-Resistant and extensively Drug-Resistant Pseudomonas aeruginosa infections. Clin Microbiol Rev, 2019. 32(4).
4. Luo Q, Lu P, Chen Y, et al. ESKAPE in China: epidemiology and characteristics of antibiotic resistance. Emerg Microbes Infect. 2024;13(1):2317915.
5. Liu YN, Zhang YF, Xu Q, et al. Infection and co-infection patterns of community-acquired pneumonia in patients of different ages in China from 2009 to 2020: a National surveillance study. Lancet Microbe. 2023;4(5):e330–9.
6. Dunphy LJ, Grimes KL, Wase N, et al. Untargeted metabolomics reveals Species-Specific metabolite production and shared nutrient consumption by Pseudomonas aeruginosa and Staphylococcus aureus. mSystems. 2021;6(3):e0048021.
7. Depke T, Thöming JG, Kordes A et al. Untargeted LC-MS metabolomics differentiates between virulent and avirulent clinical strains of Pseudomonas aeruginosa. Biomolecules, 2020. 10(7).
8. Leggett A, Li DW, Sindeldecker D, et al. Cadaverine is a switch in the lysine degradation pathway in Pseudomonas aeruginosa biofilm identified by untargeted metabolomics. Front Cell Infect Microbiol. 2022;12:833269.
9. Abdelhamid AG, Yousef AE. Untargeted metabolomics unveiled the role of butanoate metabolism in the development of Pseudomonas aeruginosa hypoxic biofilm. Front Cell Infect Microbiol. 2024;14:1346813.
10. Sumner LW, Amberg A, Barrett D, et al. Proposed minimum reporting standards for chemical analysis chemical analysis working group (CAWG) metabolomics standards initiative (MSI). Metabolomics. 2007;3(3):211–21.
11. Zhou Z, Luo M, Zhang H, et al. Metabolite annotation from knowns to unknowns through knowledge-guided multi-layer metabolic networking. Nat Commun. 2022;13. https://doi.org/10.1038/s41467-022-34537-6.
12. Wei TT, Xu W, Tu B, et al. Plasma metabonomics of human Adenovirus-infected patients with pneumonia and upper respiratory tract infection. Curr Med Sci. 2024;44(1):121–33.
13. Hornburg D, Wu S, Moqri M, et al. Dynamic lipidome alterations associated with human health, disease and ageing. Nat Metab. 2023;5(9):1578–94.
14. Grootemaat AE, van der Niet S, Scholl ER, et al. Lipid and nucleocapsid N-Protein accumulation in COVID-19 patient lung and infected cells. Microbiol Spectr. 2022;10(1):e0127121.
15. Shaikh SR, Fessler MB, Gowdy KM. Role for phospholipid acyl chains and cholesterol in pulmonary infections and inflammation. J Leukoc Biol. 2016;100(5):985–97.
16. Rong HM, Kang HY, Tong ZH. Metabolomic profiling of lungs from mice reveals the variability of metabolites in Pneumocystis infection and the metabolic abnormalities in BAFF-R-Deficient mice. J Inflamm Res. 2023;16:1357–73.
17. Chouchane O, Schuurman AR, Reijnders TDY, et al. The plasma lipidomic landscape in patients with Sepsis due to Community-acquired pneumonia. Am J Respir Crit Care Med. 2024;209(8):973–86.
18. Di Gioia M, Zanoni I. Dooming phagocyte responses: inflammatory effects of endogenous oxidized phospholipids. Front Endocrinol (Lausanne). 2021;12:626842.
19. Irún P, Gracia R, Piazuelo E, et al. Serum lipid mediator profiles in COVID-19 patients and lung disease severity: a pilot study. Sci Rep. 2023;13(1):6497.
20. Kumar S, Huang J, Abbassi-Ghadi N, et al. Mass spectrometric analysis of exhaled breath for the identification of volatile organic compound biomarkers in esophageal and gastric adenocarcinoma. Ann Surg. 2015;262(6):981–90.

21. Wu J, Cyr A, Gruen DS, et al. Lipidomic signatures align with inflammatory patterns and outcomes in critical illness. Nat Commun. 2022;13(1):6789.
22. Mitri C, Philippart F, Sacco E, et al. Multicentric investigations of the role in the disease severity of accelerated phospholipid changes in COVID-19 patient airway. Microbes Infect. 2024;26(5–6):105354.
23. Ubhi BK, Riley JH, Shaw PA, et al. Metabolic profiling detects biomarkers of protein degradation in COPD patients. Eur Respir J. 2012;40(2):345–55.
24. Engelen M, Jonker R, Thaden JJ, et al. Comprehensive metabolic flux analysis to explain skeletal muscle weakness in COPD. Clin Nutr. 2020;39(10):3056–65.
25. Suber TL, Wendell SG, Mullett SJ, et al. Serum metabolomic signatures of fatty acid oxidation defects differentiate host-response subphenotypes of acute respiratory distress syndrome. Respir Res. 2023;24(1):136.
26. Alves VB, Basso PJ, Nardini V, et al. Dehydroepiandrosterone (DHEA) restrains intestinal inflammation by rendering leukocytes hyporesponsive and balancing colitogenic inflammatory responses. Immunobiology. 2016;221(9):934–43.
27. Traish AM, Kang HP, Saad F, et al. Dehydroepiandrosterone (DHEA)--a precursor steroid or an active hormone in human physiology. J Sex Med. 2011;8(11):2960–82. quiz 2983.
28. Chatterton RT. Functions of dehydroepiandrosterone in relation to breast cancer. Steroids. 2022;179:108970.
29. Arlt W, Hammer F, Sanning P, et al. Dissociation of serum dehydroepiandrosterone and dehydroepiandrosterone sulfate in septic shock. J Clin Endocrinol Metab. 2006;91(7):2548–54.
30. Zou H, Shen Y, Li C, et al. Two phenotypes of Klebsiella pneumoniae ST147 outbreak from neonatal Sepsis with a slight increase in virulence. Infect Drug Resist. 2022;15:1–12.
31. Lopes-Pires ME, Naime AC, Almeida Cardelli NJ, et al. PKC and AKT modulate cGMP/PKG signaling pathway on platelet aggregation in experimental Sepsis. PLoS ONE. 2015;10(9):e0137901.
32. Rudiger A, Singer M. Mechanisms of sepsis-induced cardiac dysfunction. Crit Care Med. 2007;35(6):1599–608.
33. Dal-Secco D, DalBó S, Lautherbach NES, et al. Cardiac hyporesponsiveness in severe sepsis is associated with nitric oxide-dependent activation of G protein receptor kinase. Am J Physiol Heart Circ Physiol. 2017;313(1):H149–63.
34. Beloborodova NV, Olenin AY, Pautova AK. Metabolomic findings in sepsis as a damage of host-microbial metabolism integration. J Crit Care. 2018;43:246–55.

Publisher's note